TU Delft

Delft University of Technology

Document Version
Final published version

Citation (APA)
Nebrijo, J., Jünemann, R., & Rossetto, T. (2025). Collapse probability assessment of mid- and high-rise shear wall buildings under earthquake events: sensitivity to floor flexibility and damping modelling. *Bulletin of Earthquake Engineering*, *24*(2), 971-999. https://doi.org/10.1007/s10518-025-02314-7

Important note
To cite this publication, please use the final published version (if applicable).
Please check the document version above.

Copyright
In case the licence states “Dutch Copyright Act (Article 25fa)”, this publication was made available Green Open Access via the TU Delft Institutional Repository pursuant to Dutch Copyright Act (Article 25fa, the Taverne amendment). This provision does not affect copyright ownership.
Unless copyright is transferred by contract or statute, it remains with the copyright holder.

Sharing and reuse
Other than for strictly personal use, it is not permitted to download, forward or distribute the text or part of it, without the consent of the author(s) and/or copyright holder(s), unless the work is under an open content license such as Creative Commons.

Takedown policy
Please contact us and provide details if you believe this document breaches copyrights.
We will remove access to the work immediately and investigate your claim.

This work is downloaded from Delft University of Technology.

Green Open Access added to TU Delft Institutional Repository
as part of the Taverne amendment.

More information about this copyright law amendment
can be found at https://www.openaccess.nl.

Otherwise as indicated in the copyright section:
the publisher is the copyright holder of this work and the
author uses the Dutch legislation to make this work public.

Bulletin of Earthquake Engineering
https://doi.org/10.1007/s10518-025-02314-7

ORIGINAL ARTICLE

Collapse probability assessment of mid- and high-rise shear wall buildings under earthquake events: sensitivity to floor flexibility and damping modelling

Javier Nebrijo[1,2] · **Rosita Jünemann**[1,2] · **Tiziana Rossetto**[3]

Received: 8 April 2025 / Accepted: 2 November 2025
© The Author(s), under exclusive licence to Springer Nature B.V. 2025

Abstract
Tall reinforced concrete shear wall buildings used for residential purposes performed well in the 2010 Maule earthquake in Chile. Despite their good performance, in 2011 the regulations governing their design (Ministerio de Vivienda y Urbanismo 2011a, b) were changed to incorporate measures to reduce wall damage by requiring special boundary elements, along with extending the design spectrum to accommodate a broader range of soil types, among other improvements. Therefore, it is now crucial to analyse the performance of RC shear wall residential buildings designed according to the updated Chilean earthquake-resistant design standards and characterise their seismic behaviour in terms of fragility functions. However, different modelling approaches can be adopted for seismic assessment, each involving specific assumptions that significantly influence the building response. This research aims to derive the fragility of typical RC tall shear wall residential buildings in Chile located in a high seismic hazard zone, by analysing the influence of modelling assumptions on the structural response, particularly for the floor system and damping ratio, as these factors have been shown to significantly affect seismic performance. One hundred synthetic ground motion records are used to assess the seismic performance of two representative case study structures (of 9 and 17 storeys) using nonlinear time history analyses. Slight, extensive, and complete damage states are selected, and fragility curves are then derived, revealing that models utilizing shell elements to represent the floor system are more efficient and better aligned with the observed behaviour of residential buildings in Chile compared to those using elastic beam elements with rigid diaphragm constraints. Moreover, it is demonstrated that damping ratios are a highly sensitive parameter, significantly influencing the collapse probability of buildings. Therefore, the use of damping ratios from studies that better reflect real-world conditions is recommended. Overall, the results show that the studied buildings do not present a risk of collapse for spectral ordinates less than or equal to 0·5 g.

Keywords Earthquake · Collapse assessment · Fragility curve · Building modelling · Shear wall structures · Shell elements

Extended author information available on the last page of the article

Published online: 26 November 2025

1 Introduction

Chile is one of the most seismically active countries in the world. Throughout its history, it has experienced large earthquakes such as the Valdivia 9.5 Mw (1960), Algarrobo 7.8 Mw (1985), Maule 8.8 Mw (2010), Iquique 8.2 Mw (2014) and Coquimbo 8.4 Mw (2015) events, amongst others. Early advances in earthquake engineering were based on empirical observations from past earthquake events, resulting in progressively enhanced seismic design codes and practices. Over time, two main forms of mid- and high-rise reinforced concrete (RC) buildings have become popular in Chilean cities due to their perceived adequate seismic performance: (i) office buildings consisting of core shear walls and perimeter-resistant frames, with storeys composed of post-tensioning slabs to control deflections due to large spans (Gallegos et al. 2023), and (ii) residential buildings, also known "fishbone" buildings composed of a shear wall system with a high wall density and solid slabs as the floor system. This paper focuses on the latter building form, as it is a common typology in Chile and can also be found in other countries.

From 1985 to 2009, a total of 1,939 permits were granted in Chile for the construction of residential RC shear wall buildings with more than nine storeys (Massone et al. 2010). These buildings are designed following the Chilean Standard 433 (NCh433) code of 1996 (Instituto Nacional de Normalización 1996), and many were impacted by the 2010 Maule earthquake, during which they demonstrated good seismic performance, as indicated by the low number of partial collapses and only one total building collapse (Alto Río building). Nonetheless, severe damage, particularly within the first few storeys, was observed in 40 of these new buildings (2%) (Massone et al. 2010). One of the lessons from this earthquake was that although NCh 433:1996 (Instituto Nacional de Normalización 1996) referred designers to ACI 318 (1995) for additional seismic design provisions, it stipulates minimum requirements neither for wall thickness nor for special boundary element reinforcement. Such minimum requirements and others were subsequently introduced in decrees DS60 (Ministerio de Vivienda y Urbanismo 2011a) and DS61 (Ministerio de Vivienda y Urbanismo 2011b).

In this context, it is now important to understand the seismic behaviour of residential RC shear wall mid- and high-rise buildings designed according to the new Chilean earthquake-resistant design regulations, enacted after 2009, which have not yet been empirically tested by a large earthquake such as the 2010 Maule event. Thus, the first objective of this paper is to assess the seismic performance of this building type by developing fragility curves. The second objective is to examine the influence of modelling assumptions, particularly those related to the floor system and damping ratios, on the resulting fragility curves, which are highly sensitive to these assumptions (D'Ayala et al. 2015). The selection of the assumptions must balance characteristics such as accurately representing local/component response in the structure and ensuring efficiency in building response computation such that a sufficient number of simulations can be carried out to generate robust statistics.

In the Chilean context, although the seismic behaviour of RC residential shear wall buildings has been studied (Ramos and Hube 2021; Pozo et al. 2020; Vásquez et al. 2020), little research has been conducted from a probabilistic perspective in terms of fragility functions. Araya-Letelier et al. (2019) analysed a typical 16-storey office building designed under the current regulations and located in Santiago using PERFORM3D (CSI Computers and Structures Inc 2023) software. In their model, shear wall macro-elements represented the core

walls, and rigid diaphragm constraints were applied to the storeys, but elements that physically represent the floor slabs were not included. They developed a damping matrix using a hybrid approach, assigning a 2.4% damping value to the first mode, and applying Rayleigh damping of 0.1% at $0.2T_1$ and $1.5T_1$ for higher modes. The authors concluded that the building exhibited satisfactory performance because the collapse probability in 50 years (Pc_{50}) did not exceed 1%, which is the recommended threshold in ASCE7-22 (ASCE 2022). Gallegos et al. (2023) analysed the same archetype as Araya-Letelier et al. (2019) but designed for soil types B and D and seismic zones II and III. The aim was to study the effect of the site conditions on the collapse probability. For all case studies, the Pc_{50} was found to be below 1%, indicating satisfactory performance.

For the case of residential RC shear wall buildings, Cando et al. (2020) analysed in OpenSees (McKenna et al. 2000) four 20-storey building models with different floor-plan configurations and designed under the current regulations, with the aim of understanding the effect of shear wall configuration on the overall building seismic performance. Only the more flexible direction in two dimensions was analysed, with the shear walls being represented by the macro-element MVLEM (multiple vertical line element model) (Kolozvari et al. 2018) and elastic beam-column elements implemented for the floor system, assuming rigid diaphragm constraints. Rayleigh damping was set to 3.0% at $0.2T_1$ and $1.5T_1$. The Pc_{50} for all the case study buildings exceeded 1%, i.e. unsatisfactory seismic performance according to ASCE7-22 (ASCE 2022).

Echeverria et al. (2022) developed a finite element model (FEM) using DIANA (TNO 2017) software to analyse a resistant axis of an 18-storey residential building designed under the pre-2010 regulations. Shell elements were used to represent the shear walls, with non-linear behaviour assumed only for the first five storeys. The floor system was modelled using linear shell elements. A sensitivity analysis was conducted to assess the impact of various modelling considerations, including the effects of damping ratios in a Rayleigh damping model. Additionally, a fragility assessment was employed with new damage limits for different performance levels proposed.

From the literature review, several modelling assumptions emerge that warrant further testing. First, the treatment of the floor system is a key consideration. In most cases, rigid diaphragm constraints have been adopted, which presents an unrealistic scenario. When floor system flexibility is taken into account, torsional modes may significantly affect the response, as supported by empirical evidence (Lemnitzer et al. 2014). Moreover, there is no clear trend regarding the type of element used to model the floor system. Not including slab elements in the model could result in an underestimate of the level of building damage, as the slab connects the structural elements and increases the axial load demand (Ramos and Hube 2021). An intermediate approach, like using equivalent elastic frame elements, should be evaluated to see if it offers a practical way to simplify numerical models. Second, there is no clear agreement on the damping ratios used in recent studies. Echeverria et al. (2022) pointed out that damping is a sensitive factor that can significantly affect the building's response. Accurately representing damping in nonlinear models continues to be a major challenge in seismic performance assessment. Traditional Rayleigh damping has been widely criticised for its limitations in nonlinear analyses, particularly due to its dependence on the mass and stiffness matrices. Recent research (e.g., Cruz and Miranda, 2017a, b; 2021) has proposed alternative formulations that more accurately capture modal damping behaviour, although their implementation in large-scale 3D models can be computationally

demanding. Consequently, there is a pressing need for consistent modelling guidelines that align more closely with empirical observations and allow the reproduction of target modal damping ratios.

This paper seeks to contribute to the state of the art by analysing the seismic performance of one mid-rise and one high-rise residential building representative of modern Chilean design and characterise their vulnerability through fragility functions. Different damping ratios and two approaches for modelling the floor system are adopted, in order to assess the impact of these modelling assumptions on the fragility functions and building collapse probability. The novelty of this study lies in the investigation of how two key modelling assumptions, floor system flexibility and damping representation, affect the seismic fragility and collapse probability of modern Chilean RC shear-wall buildings. These are two critical aspects of structural modelling that remain insufficiently explored in the existing literature. The case study buildings are assumed, for design, to be located in Viña del Mar, an area that is among the most seismically active in the country and typified by soft soils that amplify strong ground motion. The case study buildings are modelled in 3D in OpenSees (McKenna et al. 2000). The shear walls are modelled using the macro element MVLEM-3D (Kolozvari et al. 2021). Although the study focuses on global collapse indicators, the three-dimensional modelling framework captures floor-by-floor responses, including inter-storey drifts and accelerations, allowing the assessment of higher-mode effects and non-uniform seismic demand distributions along the height, particularly relevant in flexible structures. For the seismic analysis 100 synthetic records are simulated considering a finite fault model, and the structure is simultaneously subjected to the two main components of the ground shaking. It is important to note that the study focuses on the effects of superstructure modelling assumptions on seismic fragility, and does not include explicit modelling of foundation systems or soil-structure interaction. Fragility curves are presented for the case study buildings, along with a discussion on the suitability of different modelling assumptions related to floor system representation and implemented damping ratios. Finally, recommendations are made on enhanced seismic detailing to achieve greater seismic resilience of residential RC shear wall buildings in Chile.

2 Case study buildings

According to the Chilean National Institute of Statistics (INE), 2,927 construction permits for RC buildings with more than nine storeys were issued in Chile between 2010 and 2022. Of these, 2,623 (88%) were for residential purposes, making this the predominant typology of new mid- and high-rise construction.

The case study buildings adopted in this paper are representative of the new residential buildings being constructed in Chile. Two buildings of different heights are selected: a 9-storey building (B1) to represent mid-rise buildings and a 17-storey building (B2) to represent high-rise buildings. Both buildings share identical floor plans, based on the archetypes proposed by Cando et al. (2020), and their seismic design complies with regulations NCh433 (Instituto Nacional de Normalización 2009) and DS60 (Ministerio de Vivienda y Urbanismo 2011a) and DS61 (Ministerio de Vivienda y Urbanismo 2011b). For design, the buildings are assumed to be sited in Viña del Mar, in seismic zone III with soil type D. Figure 1 shows the floor plan and 3D representations of the two case study buildings.

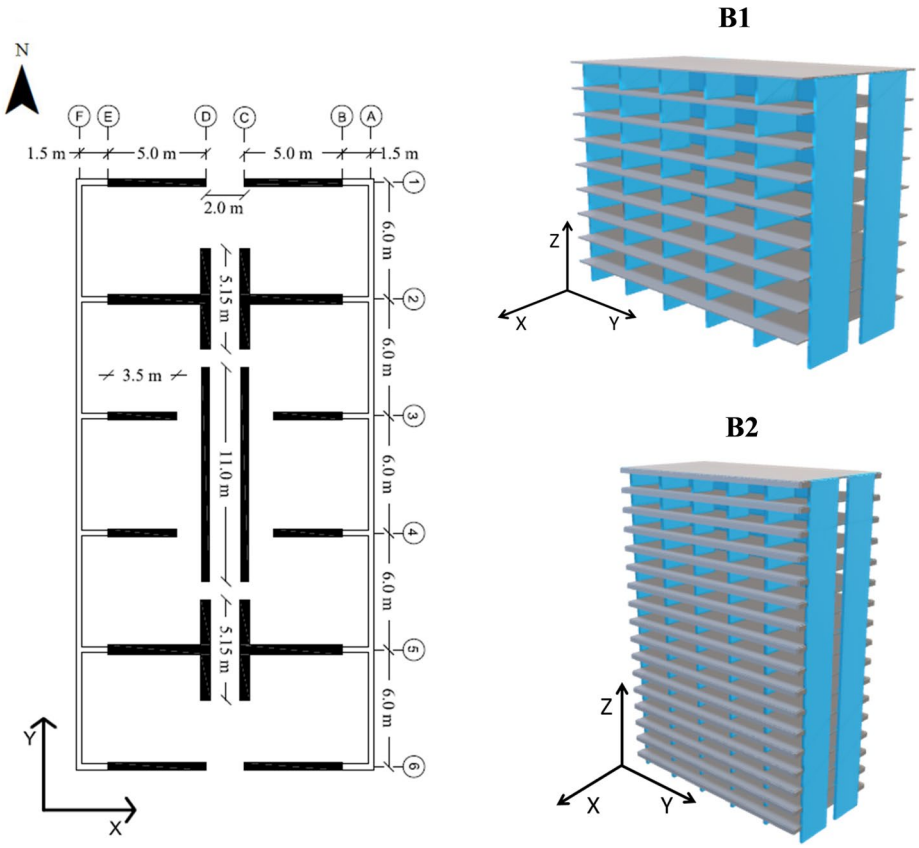


Fig. 1 Schematic drawings of the case study buildings' floorplan (left) and elevation (right). Drawings not to scale

It is important to mention that special boundary elements are not required in the design of Building B1 due to low wall deformations resulting from flexural-compression effects. In contrast, special boundary elements are required for all walls in the X direction of B2 up to the third storey, in accordance with ACI-318 (1995) recommendations. Figure 2 shows the comparison between the seismic reinforcement design of T-walls located along axes 2 and 5 in Buildings B1 and B2, highlighting the special and ordinary boundary elements. It also illustrates the measurement of wall thickness and boundary element width.

Figure 2 shows that the T-walls in Building B2 have a more robust design incorporating special boundary elements. These elements impose stricter confinement requirements on the reinforcement bars compared to ordinary boundary elements, as their primary function is to protect the wall edge bars from local buckling. The structural design of Buildings B1 and B2 is summarised in the Tables 1 and 2, respectively, where the T-walls are subdivided into their web and flange.

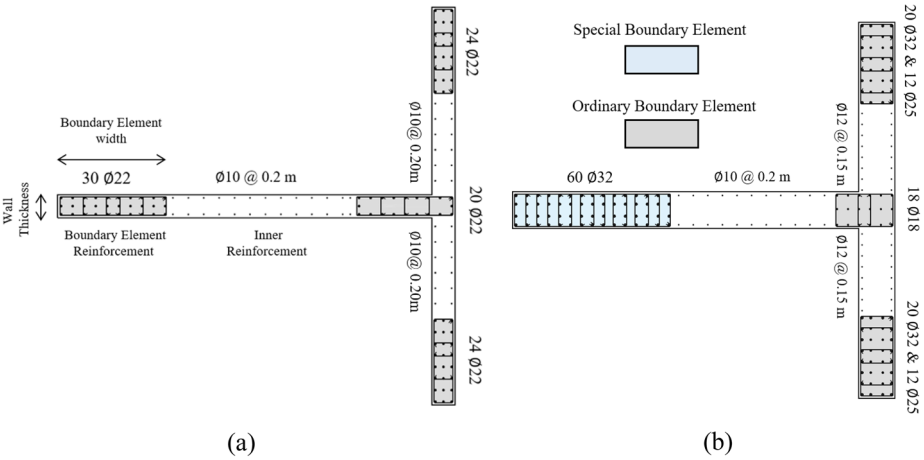


Fig. 2 Seismic reinforcement design of T-walls located along axes 2 and 5: (**a**) T-walls in building B1, (**b**) T-walls in building B2 (storeys 1–3)

Table 1 Structural design summary of building B1

Wall Axis	Between axes	Storey	Boundary Element Type	Wall Thickness	Boundary Element Reinforcement	Inner Reinforcement	Boundary Element width
1, 6	B-C, E-D	1–9	Ordinary	0.3 m	16 ϕ 22	ϕ 10 @ 0.20 m	0.95 m
2, 5	B-C, E-D	1–9	Ordinary	0.3 m	30 ϕ 22	ϕ 10 @ 0.20 m	1.44 m
3, 4	B-C, E-D	1–9	Ordinary	0.3 m	16 ϕ 20	ϕ 10 @ 0.20 m	0.95 m
C, D	1–3, 4–6	1–9	Ordinary	0.3 m	24 ϕ 22	ϕ 10 @ 0.20 m	1.16 m
C, D	2–5	1–9	Ordinary	0.3 m	30 ϕ 25	ϕ 16 @ 0.15 m	1.50 m

Slab thickness: 0.16 m

Table 2 Structural design summary of building B2

Wall Axis	Between axes	Storey	Boundary Element Type	Wall Thickness	Boundary Element Reinforcement	Inner Reinforcement	Boundary Element width
1, 6	B-C, E-D	1–3	Special	0.4 m	21 ϕ 25	ϕ 12@ 0.20 m	0.95 m
2, 5	B-C, E-D	1–3	Special	0.5 m	60 ϕ 32	ϕ 10@ 0.20 m	2.20 m
3, 4	B-C, E-D	1–3	Special	0.4 m	16 ϕ 22	ϕ 10@ 0.15 m	0.95 m
1, 6	B-C, E-D	4–17	Ordinary	0.4 m	21 ϕ 18	ϕ 12@ 0.20 m	0.95 m
2, 5	B-C, E-D	4–17	Ordinary	0.5 m	8 ϕ 25 & 36 ϕ 18	ϕ 10@ 0.20 m	1.65 m
3,4	B-C, E-D	4–17	Ordinary	0.4 m	14 ϕ 18	ϕ 10@ 0.15 m	0.95 m
C, D	1–3, 4–6	1–3	Ordinary	0.5 m	20ϕ 32 & 12 ϕ 25	ϕ 12@ 0.15 m	1.16 m
C, D	1–3, 4–6	4–17	Ordinary	0.5 m	20ϕ 28 & 12 ϕ 25	ϕ 12@ 0.15 m	1.16 m
C, D	2–5	1–17	Ordinary	0.4 m	30 ϕ 32	ϕ 16@ 0.15 m	1.50 m

Slab thickness: 0.20 m

3 Model validation

Post-earthquake reconnaissance following the 2010 Maule earthquake in Chile showed that the most common failure mechanism in Chilean residential reinforced concrete buildings was dominated by flexural-compression behaviour. Shear failure was rarely observed in typical structural walls with conventional detailing and aspect ratios (Saito et al. 2011; Westenenk et al. 2012; Saatcioglu et al. 2013). This field evidence is supported by laboratory tests on RC walls representative of Chilean construction, which also indicate that seismic damage is governed by flexural response (Chacón-Valero et al. 2025; Massone et al. 2019; Rojas et al. 2024). Based on this experimental and empirical evidence, the MVLEM-3D (Kolozvari et al. 2021) element is used in this study to model shear walls. This element is composed of vertical fibres and a horizontal linear spring defined by the shear modulus and the effective shear area of the wall cross-section. This element can represent shear walls dominated by flexural behaviour, which is the case for the case study buildings. Moreover, it is computationally efficient, making it particularly suitable for large-scale modelling and to conduct the numerous structural analyses required for the development of fragility functions. The out-of-plane behaviour of the shear walls is represented in the element through a linear Kirchhoff plate. This element has been used and validated to represent the behaviour of RC walls (Kolozvari et al. 2018, 2021). The validation is included here to support the implementation performed in this research. To this end, the RW2 and TW2 specimens from Thomsen and Wallace (Thomsen 1995) are replicated using Concrete02 (Yassin 1994) and SteelMPF (Filippou and 1983) materials for concrete and steel behaviour, respectively. The nominal material strengths such as the concrete compressive strength, nominal steel properties, and elastic modulus of materials are obtained from the experimental data (Thomsen 1995), while the remaining parameters related to the non-linear behaviour of the elements are adopted from the MVLEM command manual (Kolozvari et al. 2016).

Finally, Fig. 3 shows the experimental tests reproduced using MVLEM-3D (Kolozvari et al. 2021) in OpenSees (McKenna et al. 2000) software, demonstrating that the selected

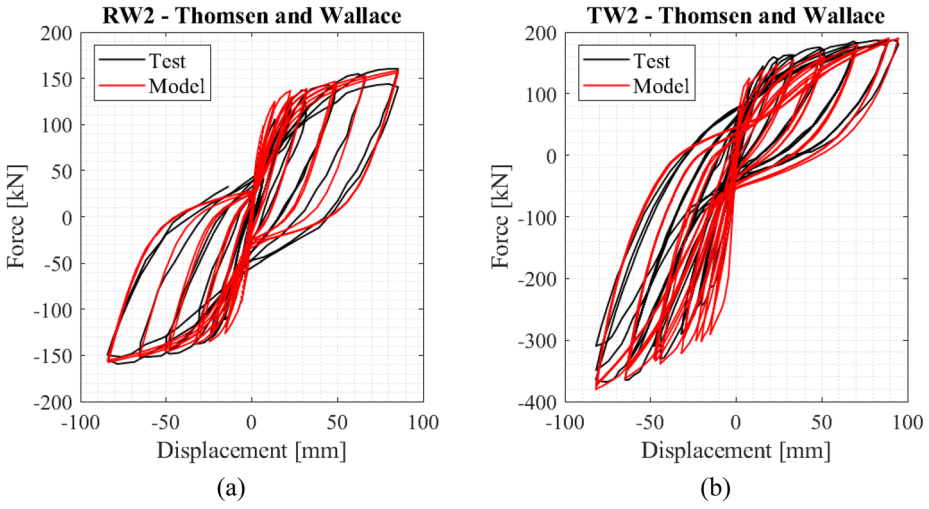


Fig. 3 Model validation: (**a**) specimen RW2, (**b**) specimen TW2

element effectively captures the response of both rectangular and T-shaped walls, aligning well with experimental results and closely resembling the finite element models reported by Echeverría et al. (2022). The model exhibits differences of 1.07% and 1.67% in maximum strength for the RW2 and TW2 specimens, respectively. Regarding total energy dissipated throughout all cycles, the differences are 7.27% for RW2 and 15.03% for TW2.

4 Model description

Based on the previous section, it can be affirmed that MVLEM-3D effectively replicates the behaviour of RC walls in buildings. Consequently, the case study buildings are modelled using this element. Following the recommendations of Cando (2020), for the analysis of residential buildings under seismic loading, Concrete02 (Yassin 1994) and Hysteretic (Scott and Filippou 2016) material models are employed to represent concrete and steel, respectively. These material models help mitigate convergence issues while maintaining result accuracy for fragility assessment. In particular, the Hysteretic (Scott and Filippou 2016) model accounts for strain hardening in steel and incorporates the effects of increased strength and strain in compression when reinforcement is confined within special boundary elements. This behaviour is implemented using the expressions proposed by Dhakal and Maekawa (2002). Moreover, a MinMax material is applied to both concrete and steel materials to enforce strain limits in compression and tension, implicitly capturing the onset of crushing and buckling failures, as suggested by Pozo et al. (2021). The structural elements are subdivided into four macro-elements per floor. Given that building deformations are highly sensitive to this discretization, material regularization is applied following the methodology of Lowes et al. (2018). This methodology directly affects the ultimate strength and strain of the concrete. Furthermore, the tensile strength of concrete is determined following the approach proposed by Wong et al. (2013). The nominal strengths adopted are $f'c = 35MPa$ for concrete and $fy = 420MPa$ for steel.

4.1 Floor system modelling

Several authors have emphasized the need for further investigation into the effect of slabs in RC buildings, as their modelling significantly influences overall building performance (Ramos and Hube 2021; Ugalde et al. 2019; Kaushik and Dasgupta 2016). Furthermore, this research seeks to contribute to the field by analysing the case study buildings following two approaches, as shown in Fig. 4: (i) incorporation of elastic beam-column (EBC) elements, following the recommendations of Cando et al. (2020). The corresponding coupling widths were selected based on the areas of the slab where the deformations due to the design lateral seismic load are concentrated. For the EBC model, rigid diaphragm constraints are assumed to link all the model nodes using the equalDOF command in combination with the constraints ('Transformation') handler. (ii) Linear ShellMITC4 elements (Dvorkin and Bathe 1984) are used to connect all the nodes across the floor plan, without imposing rigid diaphragm constraints. This modelling approach enables the consideration of torsional modes that can be excited in tall buildings under earthquake loading. The shell elements were assigned isotropic elastic membrane properties (ElasticMembranePlateSection), enabling the in-plane stiffness and deformation capacity of the floor system to be captured without

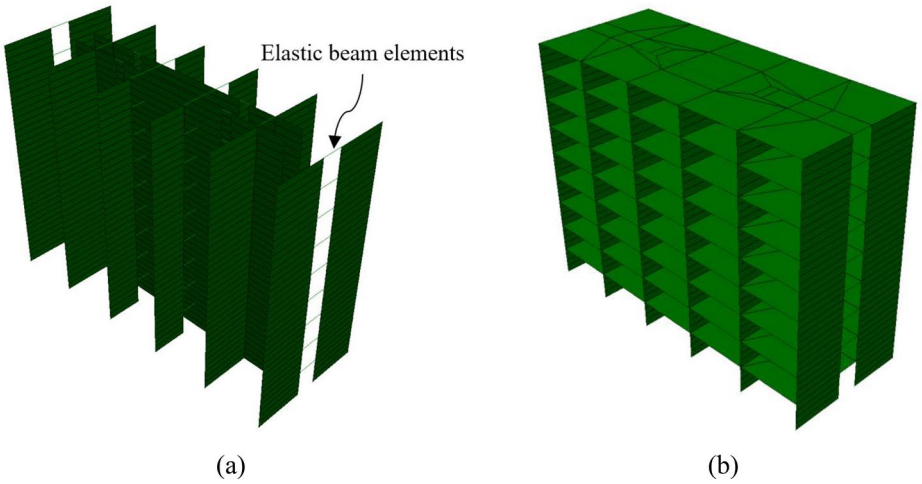


Fig. 4 Numerical model representation: (**a**) building B1 with EBC as floor system, (**b**) building B1 with ShellMITC4 as floor system (Anurag 2020)

Table 3 Modal periods and participation mass ratios for the case study building models with different floor modelling assumptions

				Modal Participation Mass Ratios [%]					
	Mode		Direction	MX	MY	MZ	RMX	RMY	RMZ
B1 ShellMITC4	1	0.408 s	X	72.12	0.0	0.0	0.0	43.05	0.0
	2	0.382 s	XY	0.0	0.0	0.0	0.0	0.0	72.04
	3	0.278 s	Y	0.0	80.07	0.0	36.06	0.0	0.0
B1 EBC	1	0.388 s	X	70.45	0.0	0.0	0.0	45.02	0.0
	2	0.273 s	Y	0.0	80.16	0.0	36.63	0.0	0.0
B2 ShellMITC4	1	1.059 s	X	69.77	0.0	0.0	0.0	37.99	0.0
	2	1.005 s	XY	0.0	0.0	0.0	0.0	0.0	71.10
	3	0.590 s	Y	0.0	77.93	0.0	29.09	0.0	0.0
B2 EBC	1	0.991 s	X	68.30	0.0	0.0	0.0	39.45	0.0
	2	0.574 s	Y	0.0	76.11	0.0	31.24	0.0	0.0

explicitly modelling cracking or nonlinearity. This simplified strategy has been employed in previous studies to evaluate diaphragm flexibility and global seismic response (e.g., Eivani et al. 2018; Lopez et al. 2024) and is considered sufficient for assessing floor-to-wall coupling and inertial force redistribution in performance-based evaluations. Nonetheless, it does not capture local slab damage mechanisms such as punching shear or in-plane cracking, which would require a non-linear layered shell formulation (Lu et al. 2015). Since both modelling assumptions are linear, the stiffness of the two floor systems is reduced by 25% in accordance with TBI guidelines (TBI 2017) to better reflect realistic flexibility. Previous studies have shown that this linear diaphragm representation, when combined with appropriate stiffness reduction factors, provides global structural responses comparable to those obtained with fully nonlinear floor system models (Ramos and Hube 2021; Lu et al. 2015).

Table 3 presents the resulting main mode characteristics for the case study buildings with the two adopted floor modelling assumptions. As expected, a torsional mode is not excited

for the EBC with a rigid diaphragm floor modelling assumption. However, the torsional mode is seen to be a significant contributor to the dynamic response of the buildings when the ShellMITC4 element is used to represent the floor system.

4.2 Damping ratios

The implementation of damping in nonlinear structural systems has been a subject of extensive debate over the years. Hall (2005) raised concerns regarding the inappropriate use of Rayleigh damping in nonlinear models, recommending the removal of the mass-proportional term and limiting the use of the stiffness-proportional component. Jehel et al. (2013) argued that employing the tangent stiffness in Rayleigh damping offers better control over the resulting modal damping ratios. Furthermore, alternative approaches for optimising Rayleigh damping coefficients have been proposed in the literature. For instance, Pan et al. (2018) introduced a methodology aimed at minimising modal damping errors, ensuring that at least one dominant mode achieves the desired damping ratio. More recently, probabilistic studies have emphasised the significant impact of damping on seismic fragility curves. Pan et al. (2020) and Wang et al. (2024) demonstrated that the damping ratio is a critical parameter affecting the probability of collapse in building structures, especially when fragility is defined based on inter-storey drift ratio thresholds. These findings reinforce the necessity of adopting damping models that more accurately reflect the dynamic characteristics of the structure. In this context, Cruz and Miranda (2017a, b; 2021) proposed new expressions for calculating modal damping ratios, applicable to both the fundamental and higher modes of vibration. Their research concluded that damping does not vary proportionally with the mass matrix and recommended the use of modal damping matrices as a more appropriate representation in the equations of motion. However, implementing this recommendation requires the full stiffness matrix, which may lead to convergence difficulties and considerably increased computational demands, particularly for large 3D building models (Scott 2019). To address these limitations, this study introduces a hybrid damping strategy. The method retains the Rayleigh damping formulation but calibrates the constants to approximate the modal damping ratios proposed by Cruz and Miranda (2017a; 2021). The damping ratio is computed as $\xi = \frac{a_0}{2\omega_n} + \frac{a_1\omega_n}{2}$, and the constants are calibrated to minimise the difference between the resulting modal damping and the target values, particularly for the first 3 modes, which contribute most significantly to the structural response. In practice, this calibration produces a good fit not only for the first three modes but also benefits the first five modes, where the modal mass participation is concentrated. Beyond this range, the discrepancies increase because of the parabolic shape inherent to the Rayleigh formulation, in contrast with the more linear trend described by Cruz and Miranda. Nevertheless, as the higher modes mobilise only a small fraction of the effective mass, these differences are expected to have negligible impact on global fragility outcomes. Additionally, Aravena and Cruz (2025) recommended limiting higher-mode damping ratios to no more than three times the damping ratio of the first mode, ensuring consistency with the frequency range identified by Cruz and Miranda (2017a). In our case, the higher-mode damping ratios remain below this limit, further supporting the adequacy of the adopted hybrid formulation. Figure 5 presents a comparison between the modal damping ratios calculated using the Cruz and Miranda (2017a; 2021) expressions, the Rayleigh damping ratios derived from the hybrid method proposed, and those obtained using the conventional approach, which in this study consists

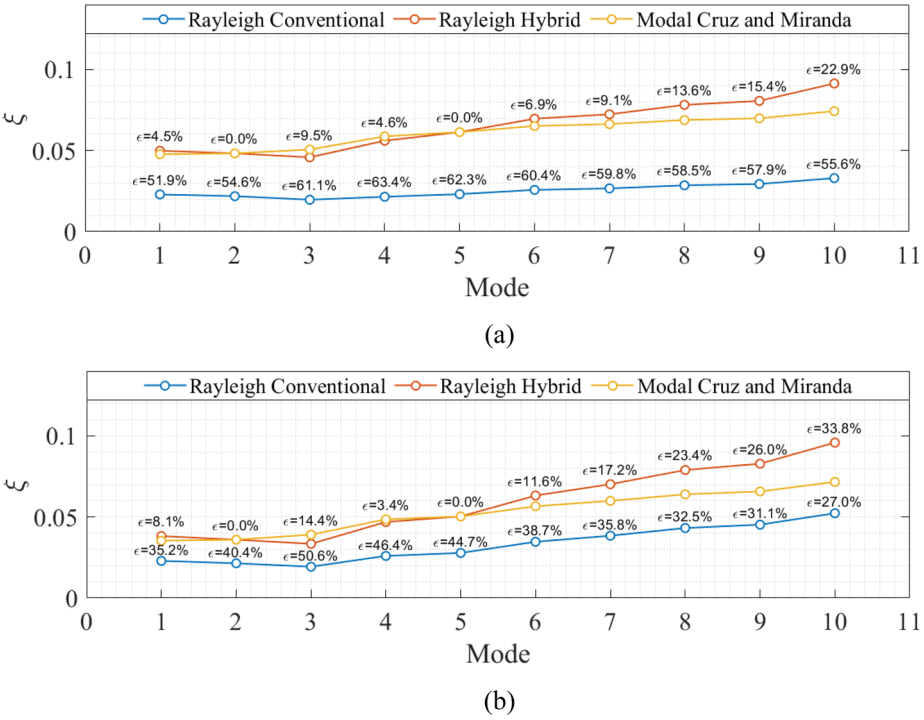


Fig. 5 Damping ratios comparison; (**a**) building B1, (**b**) building B2

of assigning a 2.0% damping ratio at two reference periods:$1.5T_1$ and $0.2T_1$. In addition, the figure shows the relative error between the conventional and hybrid Rayleigh approaches versus the modal damping ratios calculated using the Cruz and Miranda expressions. The Cruz and Miranda model is taken here as the reference target because it represents the most recent formulation supported by empirical observations. These comparisons are made for case study buildings B1 and B2 with the ShellMITC4 floor system. It is evident that, for both buildings, implementing the traditional Rayleigh damping ratios leads to an underestimation of the damping effect in the structure. Meanwhile, in the hybrid case, where greater emphasis is placed on adjusting the first 3 modes, a larger error is observed in the higher modes, exceeding 15% from the 9th and 7th modes of Buildings B1 and B2, respectively. However, as the structures responses are dominated by the first modes, this error is expected to have low impact on their fragility.

Importantly, this study presents the first application of a damping calibration strategy developed for computationally demanding three-dimensional models of Chilean mid- and high-rise shear wall buildings, within a probabilistic seismic assessment framework. By incorporating this efficient and realistic damping approach into fragility analysis, the method offers a more reliable basis for evaluating collapse risk and improves the accuracy of seismic performance predictions for complex structural systems.

5 Earthquake records

To generate fragility functions from a set of ground motion records covering a sufficiently wide range of intensity measure (IM) values while avoiding the use of large scaling factors commonly applied in conventional methodologies, this study adopts an alternative approach based on physics-based simulations. Excessive scaling can distort key characteristics of ground motions, including amplitude, duration, and spectral shape, resulting in records that no longer represent plausible earthquake scenarios (Luco and Bazzurro, 2007). Instead, synthetic ground motions are generated derived from the methods described in Estrada et al. (2025). These simulations consist of a fixed rupture area bounded between latitudes −34 and −31, and longitudes −71.05 and −73.05, representing the limits of the 2010 Maule earthquake (Cienfuegos et al. 2018) and the 2015 Illapel earthquake (Satake and Heidarzadeh 2017). The rupture is assumed to extend downward from the trench between the South American and Nazca plates to a depth of 60 km, assuming a complete rupture of the interface zone (Poulos et al. 2019). The geometry of the rupture surface is defined according to the Slab 2.0 model (Hayes et al. 2018) and a finite fault model from Crempien et al. (2020) is used to generate the spatial slip distribution conditioned to events of magnitudes between 8.5 and 9.0 Mw. Finally, 100 fault scenarios are generated. Figure 6 shows the slip distribution in the finite fault model obtained for one seismic event.

Using the results obtained from the finite fault simulations, synthetic ground motion records are calculated. The corrected empirical Green functions method is employed (Kowada et al. 1998), as it has been widely applied, including in the Chilean context (e.g., Cortez et al. 2022; Fernández et al. 2022). This method involves deriving the strong ground motion for a large earthquake event $(U_e(f))$ at a target site using an initial signal of a smaller event $(O_s(f))$ located in the fault model. In this way, Eq. (1) shows the general expression of the corrected empirical Green functions, where $U_e(f)$ is the large earthquake that depends

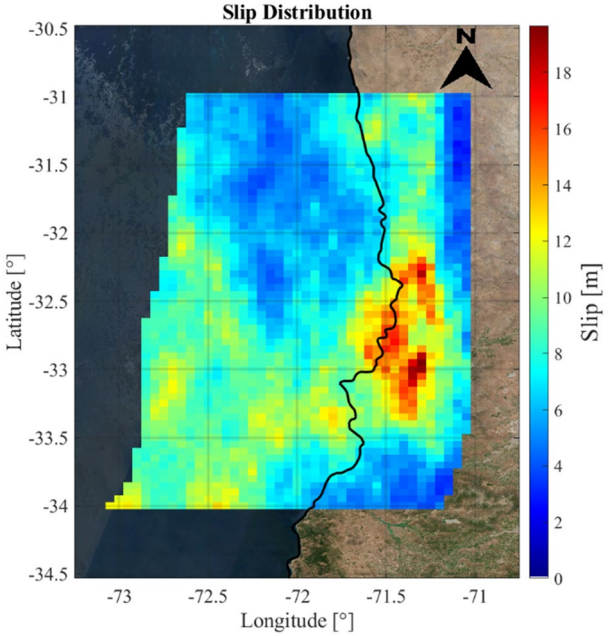


Fig. 6 Slip distribution in the finite fault model

on source effect ($|S(f)|$), path effect ($|P(f)|$), site effect ($|G(f)|$) and one initial signal ($O_s(f)$) that is a real record preferably of events with a magnitude less than 5.5 Mw to exclude the influence of non-linear soil effects (Wu et al. 2010).

$$U_e(f) = |S(f)|\,|G(f)|\,|(P(f)|\frac{O_s(f)}{|O_s(f)|} \tag{1}$$

Source effects are calculated using Eq. (2), which is constrained to follow the ω^{-2} Aki model (Aki 1967), where M_{OS} is the seismic moment of the strong motion generation areas (SMGAs), which are where the greatest energy release occurs (Fernández et al. 2022). SMGAs are selected for each fault simulation, ensuring they are 0.24 times the size of the fault plane, as recommended by Skarlatoudis et al. (2016). C is a constant calculated with Eq. (3) (Boore 1983) and depends on the average shear-wave radiation pattern coefficient ($R_{\theta\phi}$ equal to 0.63) (Fernández et al. 2022), the amplification due to the free surface condition FS (equal to 2) (Fernández et al. 2022), the partition of S-wave energy in two horizontal components $PRTITN$ (equal to 0.71) (Fernández et al. 2022), the density in the source region ρ(equal to $2.8g/cm^3$) and the shear wave velocity in the source area β (equal to $3.8km/s$) (Peyrat et al. 2010). Meanwhile, N represents the spatial and temporal discretization of the SMGA, which is set to 5 (Fernández et al. 2022), meaning that each SMGA is subdivided in a mesh of 5 × 5rectangles with a slip velocity time function discretized in 5 parts. f_{cs} is the corner frequency of the SMGA which can be calculated using Eq. (4) (Brune 1970, 1971) where S_s is the area of the SMGA.

$$|S(f)| = \frac{\frac{CM_{OS}}{N^3}}{1 + \left[\frac{f}{Nf_{cs}}\right]^2} \tag{2}$$

$$C = \frac{R_{\theta\phi} FS\ PRTITN}{4\pi\rho\beta^3} \tag{3}$$

$$f_{cs} = 0.66\frac{\beta}{\sqrt{S_s}} \tag{4}$$

Further, the path effect ($|P(f)|$) was obtained based on the relative positions of the site, the small event and the large event. The epicentres of the large and small events were randomly selected following the most likely locations shown by Mai et al. (2005). For the target site, the Casino of Viña del Mar is selected as the hypothetical location, at latitude −33.019 and longitude −71.560. Equation 5 shows the expression used to calculate the path effects, which involves a double summation over the internal sub-faults of the SMGAs, previously subdivided into a 5 × 5mesh. $1/R(r_{kl})$ represents the geometrical spreading due to path effects, obtained through Eq. (6), wherein r_{kl} is the distance between the (k,l)sub-fault and the site. The parameter t_{kl}, calculated in Eq. (7), represents the time shift resulting from differences in rupture times and the relative distances between the sub-faults and the site of interest. ξ_{kl} is the distance from the large event epicentre to the (k,l)sub-fault and ν_r is the rupture velocity, which is assumed to be equal to $2km/s$ as this velocity was observed in large events in the region (Christensen and Ruff 1986). r_e is the distance from the small

event epicentre to the site. $Q(f)$ is the quality factor, which refers to a measure of the energy attenuation of a seismic wave as it travels through the Earth, as a function of its frequency. It is calculated using Eq. (8), which was derived from empirical data according to Fernández et al. (2022).

$$|P(f)| = \sum_{k} \sum_{l} \frac{1}{R(r_{kl})} \exp\{-2\pi i f t_{kl}\} \exp\left\{-\frac{\pi f r_{kl}}{Q(f)\beta}\right\}$$

$$i = \sqrt{-1} \tag{5}$$

$$R(r_{kl}) = \begin{cases} r_{kl} & r_{kl} < 80\ km \\ \sqrt{80 r_{kl}} & r_{kl} \geq 80\ km \end{cases} \tag{6}$$

$$t_{kl} = \frac{\xi_{kl}}{\nu_r} + \frac{r_{kl} - r_e}{\beta} \tag{7}$$

$$Q(f) = 239 f^{0.71} \tag{8}$$

In addition, $|G(f)|$ is set at 1, as site effects are considered by selecting the records $O_s(f)$. Finally, the large earthquake event $(U_e(f))$ is corrected by Eq. (9) which represents the difference in slip velocity time functions between the large and small events (Irikura et al. 1997). τ_r is the rise time, which means the time it takes for a seismic wave to go from its minimum to its maximum value in the cycle of a wave; it depends on the width $(W)$of each SMGA and the rupture velocity (Fernández et al. 2022).

$$F(f) \cong 1 + \frac{(N-1)(1 - \exp(-1 - if\tau_r))}{(1 - \exp(-1))(1 + if\tau_r)}$$

$$\tau_r = \frac{1}{4}\frac{W}{\nu_r} \tag{9}$$

Figure 7 shows the seismic moment distribution in the finite fault model for the same event shown in Fig. 6, where the rectangles represent the SMGAs. The green and red markers represent the locations of the small and large event epicentres respectively, while the yellow marker represents the building location.

For the use of the initial signal $(O_s(f))$ the east-west and north-south components from a set of existing records in the Siber-Risk database (Castro et al. 2022) are randomly selected, specifically from seismic stations near the building location with a similar soil condition. Finally, by implementing the previously described procedure, a pair of the synthetic records is generated. Figure 8 shows the response spectra of the synthetic earthquake records obtained, where the red line represents the median. A well-distributed set of synthetic ground motions is obtained for each analysis direction, with higher intensities in the east–west direction, consistent with the primary motion direction of the subduction zone between the Nazca and South American plates. To provide context, Fig 8 also includes the spectra of three recorded subduction earthquakes: the 2010 Maule earthquake (Mw 8.8;

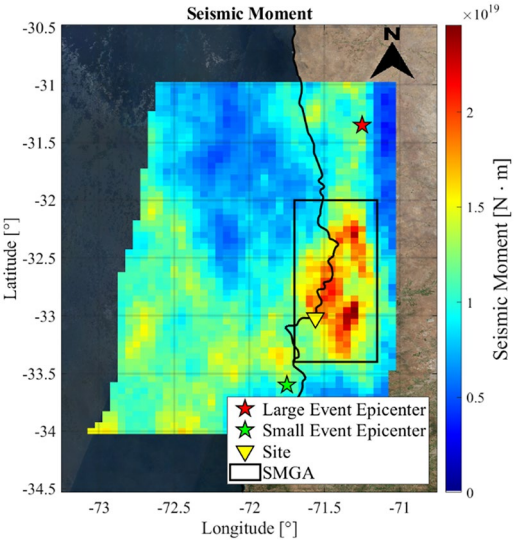


Fig. 7 Seismic moment distribution in finite fault model

Viña Centro station, RENADIC) (Centro Sismológico Nacional 2010); the 2015 Illapel earthquake (Mw 8.3; V09A station, CSN portal) (Centro Sismológico Nacional 2015), and the 1985 Valparaíso earthquake (Mw 7.8; San Isidro station, COSMOS database) (COSMOS 1985). All selected stations correspond to soil type D conditions, consistent with the geotechnical conditions of the case-study buildings. These comparisons demonstrate that the synthetic ground motions achieve a satisfactory spectral compatibility with real Chilean subduction events.

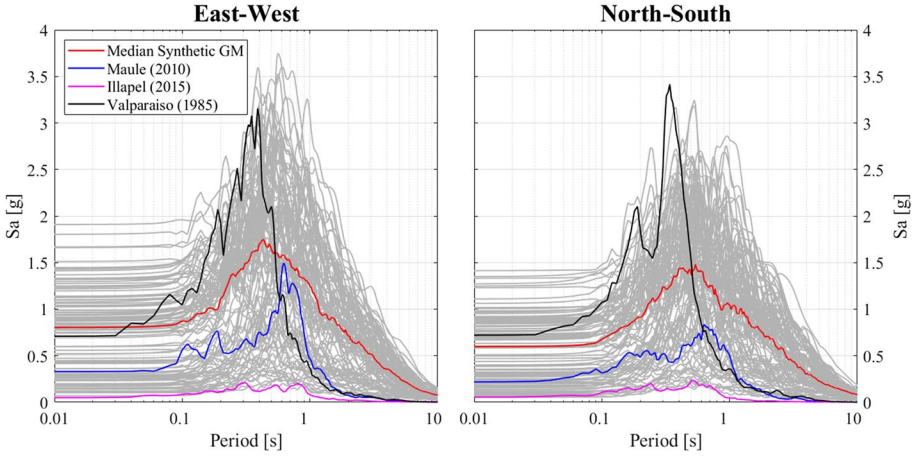


Fig. 8 Response spectra of the synthetic earthquake records

Table 4 Model identification for the cases study

Building	Model ID	Damping	Floor system
B1	M1	Conventional Rayleigh	EBC + Rigid diaphragm
	M2	Conventional Rayleigh	ShellMITC4
	M3	Hybrid Rayleigh	ShellMITC4
B2	M1	Conventional Rayleigh	EBC + Rigid diaphragm
	M2	Conventional Rayleigh	ShellMITC4
	M3	Hybrid Rayleigh	ShellMITC4

6 Results

Non-linear dynamic analyses are conducted to assess the case study buildings' seismic performance. The structures are simultaneously subjected to both perpendicular earthquake components. There are three variants for each case study building: Models M1, M2 and M3. In Model M1 the structure is modelled with an equivalent elastic beam-column system floor and rigid diaphragm constraints, adopting a conventional Rayleigh damping matrix fitted in the periods $1.5T_1$ and $0.2T_1$. In Model M2 the structure uses an elastic ShellMITC4 element as the floor system, which releases the diaphragm constraints and accounts for floor flexibility and torsional modes. A conventional Rayleigh damping matrix fitted in the periods $1.5T_1$ and $0.2T_1$ is employed. Finally, in Model M3, the structure is modelled using elastic ShellMITC4 elements for the floor system, and Rayleigh damping is implemented with coefficients calibrated to match the damping ratios proposed by Cruz and Miranda (2017a; 2021). Table 4 summarises all the analysed cases.

6.1 Inter-storey drift ratio profiles

The maximum inter-storey drift ratio (ISDR) is obtained from the 100 records for each analysis direction wherein the median values are plotted over the building height in Fig 9 for both buildings, considering the different modelling variants described in Table 4. For Building B1, the ISDR response in the east-west (X) direction is significantly larger than in the north-south (Y) direction, by nearly an order of magnitude. Model M1, with the EBC floor system, exhibits greater displacement demand in the east-west (X) direction, as omitting the translational mode concentrates the displacement demand in the most flexible direction. In addition, Model M3, using the hybrid Rayleigh approach, shows a significant reduction of nearly 50% in the ISDR response compared to the conventional Rayleigh model (M2).

In the case of Building B2, larger ISDR values are observed in the north-south (Y) direction compared to Building B1, due to the higher number of storeys. In both directions of analysis, Model M1, which uses the EBC floor system, exhibited greater displacement demand compared to Models M2 and M3, which uses the ShellMITC4 floor system. Models M2 and M3 exhibit differences, although they are less significant compared to those observed in Building B1.

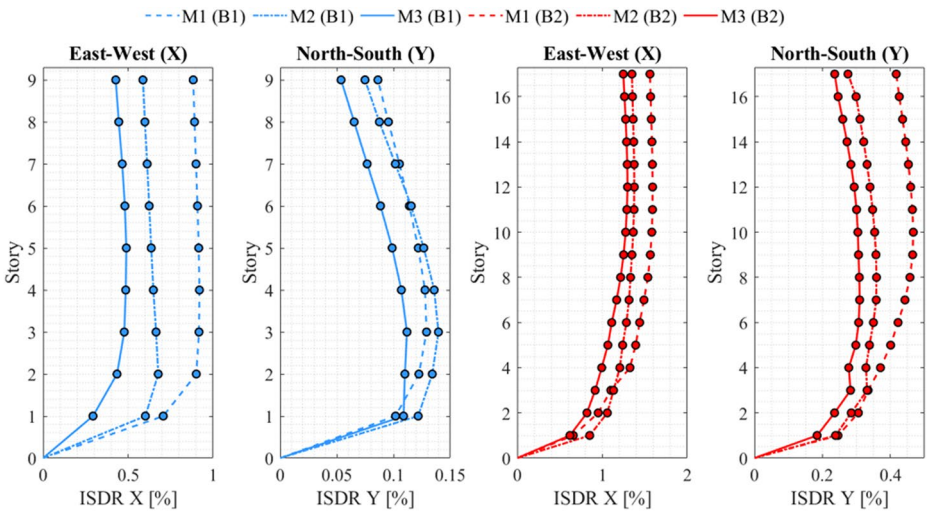


Fig. 9 Median inter-storey drift ratio profiles for case study buildings

6.2 Axial loads

The modelling assumptions regarding the floor system play an important role in the coupling of shear walls, as it transmits axial loads during an earthquake, which can significantly influence the building's damage state (Ramos and Hube 2021). At first glance, models using ShellMITC4 for the floor system exhibit a more realistic force distribution, as they allow wall coupling through slab stiffness without requiring rigid diaphragm constraints. This facilitates a more representative structural interaction, where the slab transmits both horizontal and torsional stresses to the walls. In contrast, models using EBC for the floor system only allow load transmission in the longitudinal direction of the walls, as the equivalent beams and rigid diaphragm constraints limit the overall coupling of the walls through the floor system.

Figure 10 shows the maximum axial load ratio (ALR), defined as $\frac{N}{f'cA_g}$, where N corresponds to the maximum axial load, $f'c$ is the concrete compressive strength, and A_g is the gross area of the wall. For each seismic record, the maximum axial load was measured for each wall on the first floor, and the box plot displays the results for all 100 records. Only

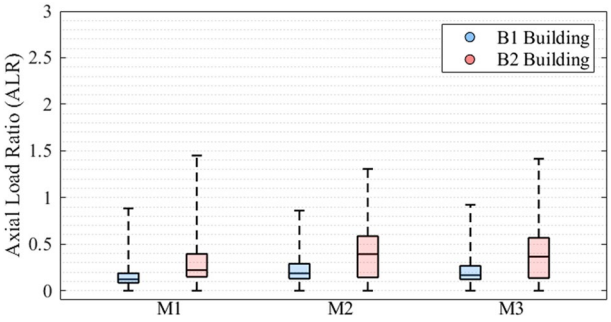


Fig. 10 Maximum axial load ratios in case study buildings

non-collapse global cases are included in this figure to reduce numerical noise and focus on meaningful fibre-level responses.

Notably, high axial load ratios are observed across all modelling assumptions, with some cases exceeding 0.35 which is the limit for ultimate loads in current Chilean regulations (Ministerio de Vivienda y Urbanismo 2011a). These exceedances are mainly related to the high axial load transfer imposed by the rigid diaphragm constraint, which, due to its linear formulation, continues to redistribute forces to the walls even after local failures occur. Nonetheless, the results show no substantial differences among the models suggesting that, for this index, all modelling assumptions exhibit similar behaviour with respect to axial load transmission.

6.3 Fragility assessment

This research considers three damage states: slight, extensive and complete. Slight damage ($ds1$), corresponding to conditions where repairs are needed but the building remains operational, is assumed when more than 55% of the structural walls in a given storey exceed the maximum cracking strain (Rossetto et al. 2016). Extensive damage ($ds2$) compromises the building's normal operation and requires major repairs, potentially including the replacement of structural elements. A structure reaching this damage state is considered uninhabitable. In the analysis of structural models, this damage state is reached when the yield deformation is exceeded in at least one fibre of 50% of the shear walls in a storey (Rossetto et al. 2016). Finally, complete damage ($ds3$) refers to severe damage that compromises the integrity of the structure, necessitating its total demolition and replacement. Based on empirical observations after the 2010 Chile earthquake (Hube et al. 2018), several shear wall buildings remained standing and were repaired even when more than one wall failed. Therefore, complete damage is considered to be achieved when more than 30% of the shear walls in one storey exceed the concrete crushing strain or the maximum steel strain in at least one fibre. This set of deformation thresholds reflects a sequential progression of damage that is consistent with the observed behaviour of Chilean wall buildings, aligning with recent experimental evidence reported by Chacón-Valero et al. (2025). Furthermore, the percentages of affected walls per storey adopted in this study are grounded in prior research (Rossetto et al. 2016) and supported by empirical observations from post-earthquake surveys (Hube et al. 2018), ensuring that the proposed criteria remain consistent with both analytical and real-world evidence.

To estimate the damage probability associated with a given intensity measure (IM), a fragility assessment is carried out. Using the damage scale, the 100 analyses are categorised following a binary approach: analyses that exceed the damage threshold are assigned a value of 1, while those that do not exceed the threshold are assigned a value of 0 (Petrone et al. 2020). A probit model is fitted to the data using the generalised linear model fitting function, *glmfit*, in MATLAB, as defined in Eq. (10), wherein DS represents the damage state of the building and dsi denotes the corresponding damage threshold. IM is the intensity measure of the earthquake record, defined by the spectral ordinate evaluated at the fundamental period of the structure ($Sa\,[T_1]$). I is a vector containing the results of the binary analysis. This function applies the maximum likelihood method, which, based on the binomial probability density function for a single experimental setup, identifies the most likely median and standard deviation through an optimisation process.

$$I = \begin{cases} 1 \; if \; DS \geq dsi \\ 0 \; if \; DS < dsi \end{cases}; glmfit\left(\log\left(IM\right), I, 'binomial', 'link', 'probit'\right) \tag{10}$$

In this way, the slope (b_2) and intercept (b_1) regression values are obtained, and the mean value (μ) and standard deviation (β) of the fragility curves are calculated from these values in accordance with Eq. (11)

$$\begin{gathered} \Phi^{-1}\left[P[DS \geq dsi|IM]\right] = b_1 + b_2 \log\left(IM\right) \\ \mu = \exp\left(-\frac{b_1}{b_2}\right) \\ \beta = \frac{1}{b_2} \end{gathered} \tag{11}$$

Figure 11 shows the fragility curves obtained for the case study buildings, with Fig 11(a) showing slight damage, Fig 11(b) showing extensive damage and Fig 11(c) presenting complete damage. In all the figures it is possible to see the significant impact of the damping ratio assumptions (M3) on the B1 fragility curves, particularly for complete damage. The use of EBC as the floor system (M1) results in higher damage probabilities than Models M2 and M3, because in this case, assuming rigid diaphragm constraints concentrates the damage in the most flexible direction (X direction), making this model more fragile than the others. However, this effect is less pronounced in the case of B2, as its increased height leads to a higher aspect ratio of the walls, causing their behaviour to be more influenced by movement in the X-direction and leading to similar performance between M1 and M2. Additionally, the complete damage fragility curve shows that no collapses were observed for $Sa\left[T_1\right] \leq 0.5g$, with the structural response being governed by flexural-compression behaviour.

The parameters of the cumulative log-normal distribution constituting the fragility functions are presented in Tables 5, 6 and 7 for slight, extensive and complete damage, respectively. In these tables, several versions of the fragility curves are presented for different intensity measures (IM), including: (i) the spectral ordinate evaluated at the fundamental period of the structure ($Sa\left[T_1\right]$) which is widely used in the Chilean context as ground motion models are typically expressed in this IM; (ii) the pseudo-acceleration average Sa_{avg}, evaluated as the geometric mean between $0.2T_1$ and $3.0T_1$ (Eads et al. 2015), which has been found to provide superior efficiency for tall buildings according to Eads et al. (2015); and (iii) the peak ground acceleration (PGA) which is commonly employed in the development of hazard maps. Given the sensitivity of collapse vulnerability to the frequency content of seismic input, $Sa\left[T_1\right]$ and Sa_{avg} are particularly suitable for mid- and high-rise buildings, as they more effectively capture the dynamic characteristics of the response compared to PGA.

Beyond the selection of intensity measures, the development of fragility functions also requires careful consideration of computational efficiency, which strongly influences decisions regarding structural modelling simplifications, analysis types, and the number of simulations needed to capture variability in both structural response and ground motion. Table 8 shows the time spent for the NLTHA using one record consisting of 25,776 time steps in

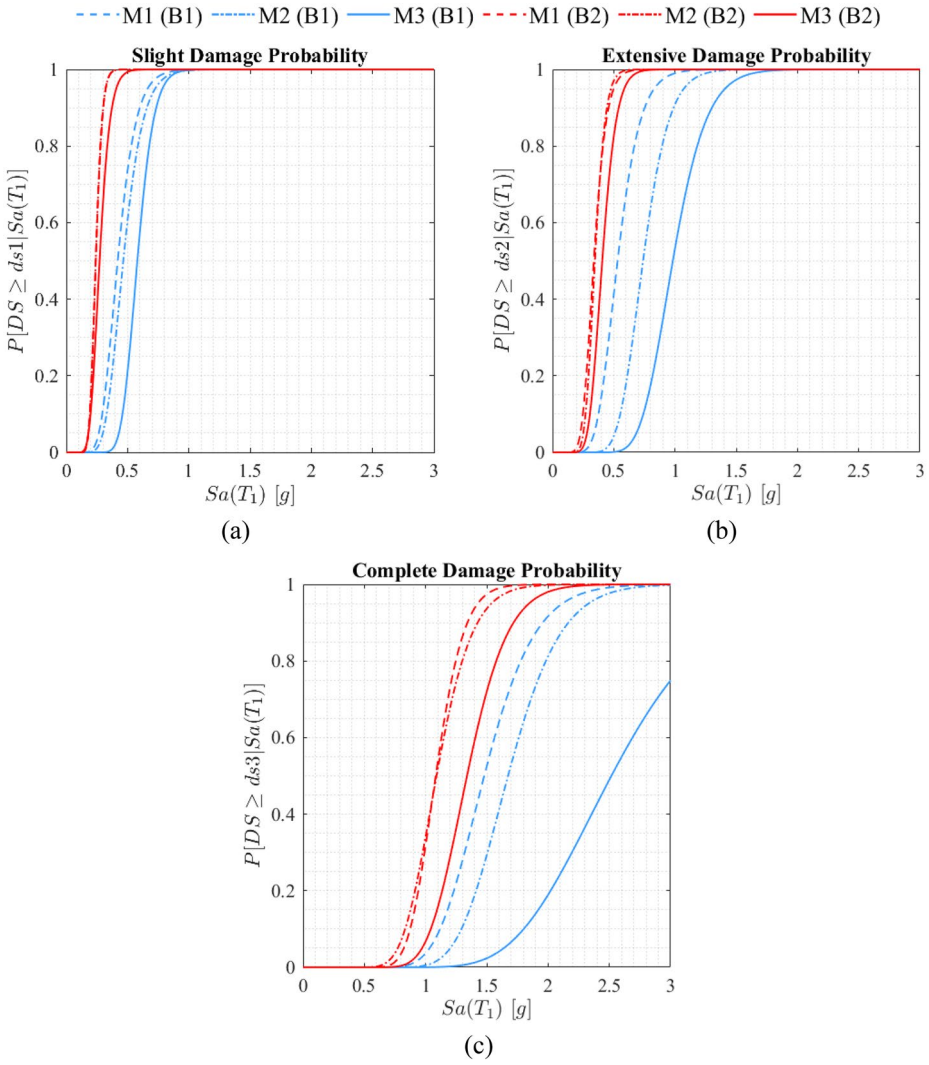


Fig. 11 Fragility curves for case study buildings: (**a**) slight damage, (**b**) extensive damage, (**c**) complete damage

Table 5 Fragility curve lognormal distribution parameters: slight damage ($ds1$)

Model ID	$Sa\,(T_1)\,[g]$		$Sa_{avg}\,[g]$		$PGA\,[g]$	
	μ [g]	β	μ [g]	β	μ [g]	β
M1 (B1)	0.4189	0.2794	0.3345	0.2512	0.1718	0.2519
M2 (B1)	0.4645	0.2705	0.3647	0.3162	0.1849	0.3173
M3 (B1)	0.5794	0.1838	0.4539	0.2606	0.2304	0.3042
M1 (B2)	0.2396	0.1765	0.1804	0.2375	0.1383	0.2289
M2 (B2)	0.2396	0.1765	0.1804	0.2375	0.1383	0.2289
M3 (B2)	0.2711	0.2468	0.2085	0.2324	0.1536	0.2886

Table 6 Fragility curve lognormal distribution parameters: extensive damage ($ds2$)

Model ID	$Sa\,(T_1)\,[g]$		$Sa_{avg}\,[g]$		$PGA\,[g]$	
	μ [g]	β	μ [g]	β	μ [g]	β
M1 (B1)	0.5312	0.2717	0.4442	0.1893	0.2212	0.2166
M2 (B1)	0.7391	0.2264	0.5736	0.2856	0.2940	0.3222
M3 (B1)	0.9821	0.2194	0.7901	0.1812	0.4122	0.2464
M1 (B2)	0.3370	0.2393	0.2623	0.1957	0.1820	0.2059
M2 (B2)	0.3461	0.1949	0.2650	0.2197	0.1915	0.2070
M3 (B2)	0.4061	0.2227	0.3179	0.1916	0.2288	0.2721

Table 7 Fragility curve lognormal distribution parameters: complete damage ($ds3$)

Model ID	$Sa\,(T_1)\,[g]$		$Sa_{avg}\,[g]$		$PGA\,[g]$	
	μ [g]	β	μ [g]	β	μ [g]	β
M1 (B1)	1.4793	0.2181	1.2890	0.1525	0.7141	0.2640
M2 (B1)	1.6737	0.2012	1.3661	0.1792	0.7559	0.3711
M3 (B1)	2.5173	0.2611	1.9640	0.1718	1.3919	0.4868
M1 (B2)	1.0832	0.1672	0.8562	0.1098	0.6424	0.3273
M2 (B2)	1.0901	0.2090	0.8667	0.0655	0.7242	0.2623
M3 (B2)	1.3388	0.1948	1.0158	0.1010	0.8907	0.3062

Table 8 Computational cost

	B1			B2		
	M1	M2	M3	M1	M2	M3
hours	106.07	11.34	10.99	859.20	21.73	21.83

both component directions. This record does not result in a complete damage state ($ds3$) for any of the modelling assumptions. The analyses are carried out in an Intel Core i5 processor with a peak velocity of 3.75 GHz. The results indicate that modelling assumption M1 requires the greatest computational time, suggesting that it is the least efficient approach for 3D building modelling. Importantly, this limitation is not related to numerical convergence, but to the high computational demand inherent to this strategy. Although the use of the 'UmfPack solver' was tested and did not present convergence problems, it substantially increased RAM memory requirements, exceeding the available hardware capacity and making large-scale, multi-processor analyses impractical. A possible workaround would be to reduce the number of parallel simulations to keep computational demand consistent with the available resources.

6.4 Deriving collapse probabilities

To calculate collapse probabilities for the buildings, the building fragility should be combined with the seismic hazard occurring within a specific mean return period. Hence, a probabilistic seismic hazard analysis (PSHA) for the site of interest is performed using the SeismicHazard toolbox (Candia et al. 2019), together with the seismicity model defined by Poulos et al. (2019). The ground motion prediction equations (GMPEs) of Idini et al. (2017) and Montalva et al. (2017) are implemented, as they represent the most recent models spe-

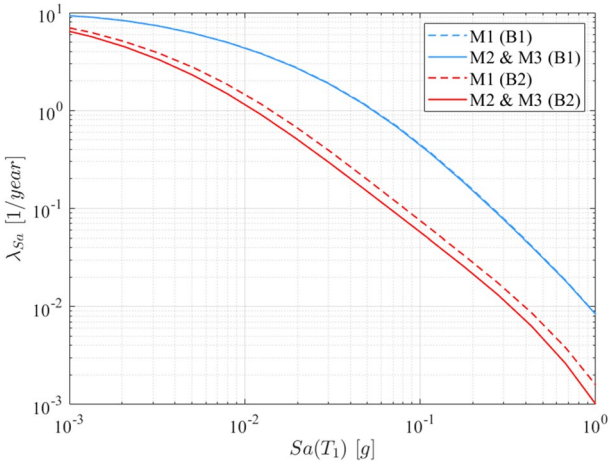


Fig. 12 Hazard curves

Table 9 Collapse probability in 50 years

B1			B2		
M1	M2	M3	M1	M2	M3
$P_C\,(50_{yrs})$ 15.2%	11.1%	4.3%	4.6%	2.9%	1.5%

cifically developed under Chilean conditions. The epistemic uncertainties are considered through a logic tree with equal weights of 0.5 for each model. Figure 12 shows the hazard curves obtained in terms of Sa(T_1), where the blue and red lines represent Buildings B1 and B2, respectively.

The mean annual frequency of collapse (λ_c) is then obtained for each case study building in accordance with Eq. (12), where $\frac{d\lambda_{Sa}}{dSa}$ is the derivative of the seismic hazard curve. Considering a classical Poisson model, as shown in Eq. (13), it is possible to obtain the collapse probability in a time window (Tw).

$$\lambda_c = \int_0^\infty P\left[DS \geq ds3 | Sa\left(T_1\right)\right] \cdot \left|\frac{d\lambda_{Sa}}{dSa}\right| \cdot dSa \tag{12}$$

$$P_C\left(Tw\right) = 1 - \exp\left(-\lambda_c \cdot Tw\right) \tag{13}$$

In this way, collapse probability for $Tw = 50\ years$ is calculated, with the results presented in Table 9. They clearly show that the use of a flexible diaphragm (Models M2 and M3) reduces the collapse probability for both B1 and B2. It is evident that the choice of Rayleigh damping has a significant influence on the collapse probabilities, with the hybrid Rayleigh damping resulting in lower collapse probabilities for both case studies. Meanwhile, the mid-rise Building B1 exhibits a higher collapse probability than the high-rise Building B2. This can be attributed to the fact that, according to design regulations, B1 did not require special boundary elements, which increases the likelihood of flexural-compression failure in this type of structure.

The M3 models align more closely with the expected results, as they incorporate refined assumptions that better represent the physical conditions of the buildings. Moreover, their

outcomes are consistent with recent findings reported in other studies on RC residential buildings (Cando et al. 2020; Vásquez and Heresi 2024). In contrast, these results tend to be higher than those observed in office buildings, which in most cases exhibit values below 1%, indicating satisfactory performance according to the ASCE performance guidelines (ASCE 2022). It is important to note, however, that Chilean seismic design codes do not specify an explicit collapse probability threshold comparable to that in ASCE 7–22. Instead, the Chilean provisions qualitatively require that structures be designed to resist severe earthquakes without collapse (Instituto Nacional de Normalización 2009). From this perspective, the findings provide insights into the potential range of collapse risk in Chilean residential buildings, framed within a distinct design philosophy and seismic context compared with that assumed in U.S. codes.

7 Conclusions

A seismic performance assessment following a probabilistic approach is conducted for mid-rise (9 storey) and high-rise (17 storey) RC shear wall buildings. These buildings are designed to meet the current seismic design regulations in Chile and are representative of modern residential buildings. Based on the current state of the art, this research has two main objectives: (i) to characterize the mid- and high-rise residential buildings through fragility curves; and (ii) to assess the impact of modelling assumptions, specifically the influence of floor system modelling and damping ratio assumptions on seismic performance. To explore these aspects, three different models of each case study building were developed, considering both rigid and flexible floor systems, as well as classical and hybrid Rayleigh damping. The hybrid damping ratios proposed in this study involves adjusting the Rayleigh constants a_0 and a_1 to match damping ratios derived from previous studies based on empirical measurements. All the models are analysed through non-linear time history analyses using 100 synthetic ground motion records. Fragility curves and collapse probabilities are then derived for each analysed building model. It is found that typical tall shear wall buildings do not present a risk of collapse for $Sa\,[T_1] \leq 0.5g$.

Although this study does not explicitly account for epistemic uncertainty through statistical variation of material properties or geometric configurations, it does address modelling-related uncertainty by exploring different structural configurations and modelling assumptions related to the superstructure. The scope of the analysis is also limited by the number of case study buildings and the range of modelling parameters considered. Additionally, foundation systems and soil-structure interaction effects are not explicitly modelled. Nevertheless, the findings provide valuable insights into the influence of key modelling decisions on seismic fragility, and support a number of conclusions and recommendations that can inform future research and improve the representation of structural behaviour in fragility assessments.

The most reliable modelling approach of those considered for assessing the seismic response of mid to high-rise residential RC shear wall buildings in Chile is that which uses the MVLEM-3D element for shear walls and ShellMITC4 elements for the floor systems. This approach is effective because, according to empirical evidence (Lemnitzer et al. 2014), torsional modes contribute significantly to the building response, and they can only be appropriately captured using a flexible floor system. This effect is particularly pronounced

in low- and mid-rise buildings, where the aspect ratio of the walls reduces the dominance of the response in one of the main directions.

The adoption of a flexible floor system also improves computational efficiency. In contrast, modelling a rigid diaphragm using the equalDOF command, particularly when combined with the constraints ('Transformation') handler, can increase computational cost. This is because a transformation matrix is introduced by this approach to enforce kinematic relationships between degrees of freedom, which must be applied and updated at each analysis step. While this can reduce the number of degrees of freedom, the repeated modification of global matrices during the analysis introduces significant computational overhead.

It is also observed that building models using hybrid Rayleigh damping ratios exhibit lower collapse probabilities compared to those using conventional Rayleigh damping. This is because conventional Rayleigh underestimates the modal damping ratios, leading to greater element deformations and a greater damage state. While the effects of damping ratios remain an active area of investigation, it is advisable to adhere to the recommendations based on empirical evidence from recent research (Cruz and Miranda 2017a; Cruz and Miranda 2021). This approach will help reduce uncertainty associated with modelling assumptions.

The results of this study indicate that the 50-year collapse probability for the mid-rise building is greater than for the high-rise building, which may seem counterintuitive. However, this can be explained by the lack of special boundary elements in the shear walls of the mid-rise building, as they are not required by the current Chilean seismic code. In the mid-rise building, damage is concentrated in the wall exterior fibres and the first storeys. It is therefore recommended that special boundary elements be included in the design of mid-rise RC shear wall buildings in order to improve their seismic resilience. While this recommendation is particularly relevant for slender walls and for seismic conditions similar to those in Chile, it is not intended as a direct modification to international codes such as ACI 318, which already prescribe boundary confinement through capacity design principles. Rather, it highlights the need to carefully consider boundary detailing in regions of high seismicity where similar structural configurations and code provisions are in place, as the associated collapse risks may otherwise be underestimated.

The fragility characterization was performed for both mid-rise and high-rise residential buildings, revealing significant sensitivity to the modelling assumptions tested. This study highlights the need for further improvements in modelling techniques to develop mathematical models that better reflect real structural behaviour and reduce the uncertainty introduced by assumptions in the modelling process. In particular, future research should consider analysing the non-linearity of slab elements, as the floor system in typical Chilean residential buildings plays a critical role in coupling structural components. Slab cracking during seismic events reduces this coupling effect, potentially altering axial load distribution and significantly impacting collapse probability.

7.1 Limitations

This study focuses on the super-structure response domain and does not explicitly model soil-structure interaction or nonlinear foundation behaviour. Nevertheless, several geotechnical effects such as local soil amplification and frequency-dependent seismic demand are indirectly addressed through the use of synthetic ground motions derived from finite-fault

rupture models and empirical Green's functions for soft soil sites. While dynamic soil properties, aftershock sequences, and cumulative damage mechanisms are beyond the scope of this work, the use of site-specific seismic input and comparative structural modelling strategies provides insight into collapse vulnerability under realistic ground motion conditions. In addition, we acknowledge that the implementation of damping models remains a source of epistemic uncertainty, particularly regarding the damping ratios of higher modes. Although the adopted hybrid approach improves the representation of the first modes, discrepancies at higher modes reflect the limitations of Rayleigh-based formulations and should be considered when interpreting the results. Furthermore, epistemic uncertainty related to material and geometric variability (e.g., concrete strength, wall thickness) was not explicitly considered, as the primary objective was to isolate the influence of modelling assumptions under a fixed design. Changing these parameters would modify the building design itself, not just its response, and therefore falls outside the scope of this study. While this choice allowed us to directly compare modelling strategies, it also implies that the results should be interpreted as conditional on the assumed design parameters

Acknowledgements The authors acknowledge funding from the National Agency of Research and Development (ANID) under the National Doctoral Scholarship 21220567 and ANID/FONDEF under grant IT23I0106, ANID/Anillo ACT240044 and CIGIDEN, ANID/FONDAP 2023/1523A0009, and the project EASER (Evolution Assessment of Seismic Risk) project under grant number ACT240044. The authors also extend their sincere gratitude to EPICentre and University College London (UCL) for providing the facilities and support necessary for the development of this work.

Author contributions All authors contributed to the study's conception and design. J. Nebrijo, R. Jünemann, T. Rossetto performed material preparation, data collection, and analysis. J. Nebrijo wrote the first draft of the manuscript, and all authors revised the manuscript and contributed to the final version. All authors read and approved the final manuscript.

Funding The doctoral studies of the first author have been financially supported by Chile's National Agency for Research and Development (ANID) through the National Doctoral Scholarship (21220567). Further support was provided by the Research Centre for Integrated Disaster Risk Management (CIGIDEN) ANID FONDAP (1523A0009).

Data availability The datasets generated during the current study are available from the corresponding author upon reasonable request.

Declarations

Declaration of generative AI and AI-assisted technologies in the writing process During the preparation of this work the author(s) used ChatGPT in order to improve the redaction. After using this tool/service, the author(s) reviewed and edited the content as needed and take(s) full responsibility for the content of the publication.

Competing interests The authors have no relevant financial or non-financial interests to disclose.

References

ACI Committee 318 (1995) Building code requirements for structural concrete : (ACI 318-95); and commentary (ACI 318R-95). American Concrete Institute, Farmington Hills

Aki K (1967) Scaling law of seismic spectrum. J Geophys Res 72(4):1217–1231

Anurag U (2020) Patent No. MIT. https://orcid.org/0000-0001-9525-5062
Araya-Letelier G, Parra PF, Lopez-Garcia D, Garcia-Valdes A, Candia G, Lagos R (2019) Collapse risk assessment of a Chilean dual wall-frame reinforced concrete office building. Eng Struct 183:770–779
ASCE (2022) Minimum design loads and associated criteria for buildings and other structures ASCE/SEI 7-22. American Association of Civil Engineers, Reston, VA, USA
Aravena A, Cruz C (2025) Effect of Variability in Damping Ratios on the Seismic Riskof Steel Moment-Frame Buildings. Earthq Eng Struct Dyn 54(8). https://doi-org.pucdechile.idm.oclc.org/10.1002/eqe.4349
Boore D (1983) Stochastic simulation of high-frequency ground motions based on seismological models of the radiated spectra. Bull Seismol Soc Am 6A(73):1865–1894
Brune JN (1970) Tectonic stress and the spectra of seismic shear waves from. J Geophys Res 75(26):4997–5009
Brune JN (1971) Correction. J Geophys Res 76(20):5002
Candia G, Macedo J, Jaimes MA, Magna-Verdugo C (2019) A new state-of-the-art platform for probabilistic and deterministic seismic hazard assessment. Seismol Res Lett 90(6):2262–2275
Cando A (2020) Efectos de la rigidez en el desempeño sísmico de edificios estructurados con muros de hormigon armado. Repositorio Pontificia Universidad Catolica de Chile, Santiago de Chile
Cando MA, Hube MA, Parra PF, Arteta CA (2020) Effect of stiffness on the seismic performance of code-conforming reinforced concrete shear wall buildings. Eng Struct 219(110724)
Castro S, Benavente R, Crempien J, Candia G, de la Llera J (2022) A consistently processed strong-motion database for Chilean earthquakes. Seismol Res Lett 93(5):2700–2718
Centro Sismológico Nacional (2010) Record of the Maule earthquake Mw 8.8, Viña Centro station (Plaza Vergara), February 27, 2010. Retrieved from https://terremotos.ing.uchile.cl/registros/164
Centro Sismológico Nacional (2015) Record of the Illapel earthquake Mw 8.3, station V09A, September 16, 2015. Retrieved from https://evtdb.csn.uchile.cl/event/6c5752b76db0f46280949a79864bef6e
Chacón-Valero E, Hube MA, Santa María H (2025) Seismic performance of damaged slender reinforced concrete walls with unconfined boundaries. J Build Eng 101. https://doi.org/10.1016/j.jobe.2025.111819
Christensen DH, Ruff LJ (1986) Rupture process of the March 3, 1985 Chilean earthquake. Geophys Res Lett 13(8):721–724
Cienfuegos R, Catalán P, Urrutia A, Benavente R, Aránguiz R, González G (2018) What can we do to forecast tsunami hazards in the near field given large epistemic uncertainty in rapid seismic source inversions? Geophys Res Lett 45(10):4944–4955
Cortez C, Jünemann R, Fernández C, Urrutia A, Crempien J, Cienfuegos R (2022) Performance of an rc building under seismic and tsunami actions in sequence via nonlinear dynamic analysis including soil-structure interaction. Eng Struct 272
COSMOS (1985) Record of the Valparaíso earthquake Mw 7.8, San Isidro station. Retrieved from https://www.strongmotioncenter.org/vdc/scripts/event.plx?evt=151#1348
Crempien J, Urrutia A, Benavente R, Cienfuegos R (2020) Effects of earthquake spatial slip correlation on variability of tsunami potential energy and intensities. Sci Rep 10:8399
Cruz C, Miranda E (2017a) Evaluation of damping ratios for the seismic analysis of tall buildings. J Struct Eng 143(1)
Cruz C, Miranda E (2017b) Evaluation of the Rayleigh damping model for buildings. Eng Struct 138:324–336
Cruz C, Miranda E (2021) Damping ratios of the first mode for the seismic analysis of buildings. J Struct Eng 147(1)
CSI Computers and Structures Inc (2023) Perform 3D, Version 7.0
D'Ayala D, Meslem A, Vamvatsikos D, Porter K, Rossetto T, Silva V (2015) Guidelines for analytical vulnerability assessment - low/Mid-rise. Global Earthquake Model
Dhakal RP, Maekawa K (2002) Modeling for postyield buckling of reinforcement. J Struct Eng 128(9)
Dvorkin E, Bathe KJ (1984) A continuum mechanics based four-node shell element for general nonlinear analysis. Eng Comput 1(1):77–88
Eads L, Miranda E, Lignos DG (2015) Average spectral acceleration as an intensity measure for collapse risk assessment. Earthq Eng Struct Dyn 44(12):2057–2073
Echeverría MJ, Junemann R, Liel AB (2022) Seismic fragility assessment of medium-rise fishbone-type reinforced concrete wall buildings. J Build Eng 59
Eivani H, Moghadam A, Aziminejad A, Nekooei M (2018) Seismic response of plan-asymmetric structures with diaphragm flexibility. Shock Vibr. https://doi.org/10.1155/2018/4149212
Estrada MF, Cienfuegos R, Urrutia A, Catalán P, Winckler P (2025). Forward energy grade line analysis for tsunami inundation mapping. Coastal Engineering
Fernández C, Nozu A, Crempien J, De la Llera J (2022) Simulation of pulse-like ground motions during the 2015 mw 8.3 illapel earthquake with a new source model using corrected empirical Green's functions. Seismol Res Lett 93(1):76–90

Filippou, Popov, Bertero (1983) Effects of bond deterioration on hysteretic behavior of reinforced concrete joints. Earthquake Engineering Research Center, University of California, Berkeley
Gallegos M, Araya-Letelier G, Lopez-Garcia D, Parra PF (2023) Collapse assessment of mid-rise RC dual wall-frame buildings subjected to subduction earthquakes. Buildings 13(4):880
Hall JF (2005) Problems encountered from the use (or misuse) of Rayleigh damping. Earthq Eng Struct Dyn 35:525–545. https://doi-org.pucdechile.idm.oclc.org/10.1002/eqe.541
Hayes G, Moore G, Portner D, Hearne M, Flamme H, Furtney M, Smoczyk G (2018) Slab2, a comprehensive subduction zone geometry model. Science 362(6410):58–61
Hube MA, Gálvez HA, Jünemann R, Elwood K (2018) Repaired reinforced concrete wall buildings in Chile after 2010 maule earthquake. In: Eleventh U.S. National Conference on Earthquake Engineering, Los Angeles, California
Idini B, Rojas F, Ruiz S (2017) Ground motion prediction equations for the Chilean subduction zone. Bull Earthq Eng 15(5):1853–1880
Instituto Nacional de Normalización (1996) NCh433.Of96: earthquake resistant design of buildings. Chile, Santiago
Instituto Nacional de Normalización (2009) Diseño de edificios resistentes a terremotos (NCh 433. Of1996) Mod. en 2009. Chile
Irikura K, Kagawa T, Sekiguchi H (1997) Revision of the empirical Green's function method by Irikura (1986). In: Seismological Society of Japan Fall Meeting, No.2, B25 (in Japanese)
Jehel P, Léger P, Ibrahimbegovic A (2013) Initial versus tangent stiffness-based Rayleigh damping in inelastic time history seismic analyses. Earthq Eng Struct Dyn 43:467–484. https://doi.org/10.1002/eqe.2357
Kaushik S, Dasgupta K (2016) Seismic damage in shear wall-slab junction in RC buildings. Procedia Eng 144:1332–1339
Kolozvari K, Kalbasi K, Orakcal K, Wallace W (2021) Three-dimensional model for nonlinear analysis of slender flanged reinforced concrete walls. Eng Struct 236(112105)
Kolozvari K, Orakcal K, Wallace J (2016) OpenSees. Retrieved 03 26, 2025, from https://opensees.berkeley.edu/wiki/index.php/MVLEM_-_Multiple-Vertical-Line-Element-Model_for_RC_Walls
Kolozvari K, Orakcal K, Wallace JW (2018) New opensees models for simulating nonlinear flexural and coupled shear-flexural behavior of RC walls and columns. Comput Struct 196:246–262
Kowada A, Tai M, Iwasaki Y, Irikura K (1998) Evaluation of horizontal and vertical strong ground motions using empirical site-specific amplification and phase characteristics. J Struct Constr Eng 63:97–104
Lemnitzer A, Massone L, Skolnik D, de la Llera JC, Wallace J (2014) Aftershock response of rc buildings in Santiago, Chile, succeeding the magnitude 8.8 Maule earthquake. Eng Struct 76:324–338
Lopez JS, Ramirez BG, Pettit C, Cruz-Noguez C (2024) Performance of simplified damage-based concrete models in seismic applications. Am J Civ Eng 12(4):95–107. https://doi.org/10.11648/j.ajce.20241204.11
Lowes L, Lehman D, Baker C (2018) Recommendations for modeling the nonlinear response of slender reinforced concrete walls using PERFORM-3D. In: Conference: SEAOC 2016
Lu X, Xie L, Guan H, Huang Y, Lu X (2015) A shear wall element for nonlinear seismic analysis of super-tall buildings using OpenSees. Finite Elem Anal Des 98:14–25. https://doi.org/10.1016/j.finel.2015.01.006
Luco N, Bazzurro P (2007) Does amplitude scaling of ground motion records result in biasednonlinear structural drift responses? Earthq Eng Struct Dyn 36(13), 1813–1835
Mai M, Spudich P, Boatwright J (2005) Hypocenter locations in finite-source rupture models. Bull Seismol Soc Am 95(3):965–980
Massone LM, Bonelli P, Lagos R, Lüders C, Moehle J, Wallace JW (2010) Seismic design and construction practices for RC structural wall buildings. Earthq Spectra 28(1):245–256
Massone LM, Muñoz G, Rojas F (2019) Experimental and numerical cyclic response of RC walls with openings. Eng Struct 178:318–330. https://doi.org/10.1016/j.engstruct.2018.10.038
McKenna F, Fenves F, Scott M (2000) Open system for earthquake engineering simulation. University of California, Berkeley
Ministerio de Vivienda y Urbanismo (2011a) Código de diseño de hormigón armado (DS 60).Chile
Ministerio de Vivienda y Urbanismo (2011b) Codigo de diseño sísmico (DS 61). Chile
Montalva GA, Bastías N, Rodriguez-Marek A (2017) Ground-motion prediction equation for the Chilean subduction zone. Bull Seismol Soc Am 107(2):901–911
Pan D, Chen G, Gao L (2016) A constrained optimal Rayleigh damping coefficients for structures with closely spaced natural frequencies in seismic analysis. Adv Struct Eng 20(1):81–95. https://doi.org/10.1177/1369433216646007
Pan H, Tian L, Fu X, Li H (2020) Sensitivities of the seismic response and fragility estimate of a transmission tower to structural and ground motion uncertainties. J Constr Steel Res 167. https://doi.org/10.1016/j.jcsr.2020.105941

Petrone C, Rossetto T, Baiguera M, De la Barra C, Ioannou I (2020) Fragility functions for a reinforced concrete structure subjected to earthquake and tsunami in sequence. Eng Struct 205
Peyrat S, Madariaga R, Buforn E, Campos J, Asch G, Vilotte JP (2010) Kinematic rupture process of the 2007 Tocopilla earthquake and its main aftershocks from teleseismic and strong-motion data. Geophys J Int 3(182):1411–1430
Poulos A, Monsalve M, Zamora N, de la Llera JC (2019) An updated recurrence model for Chilean subduction seismicity and statistical validation of its poisson nature. Bull Seismol Soc Am 109(1):66–74
Pozo J, Hube M, Kurama Y (2020) Quantitative assessment of nonlinear macro-models for global behavior and design of planar RC walls. Eng Struct 224(111190)
Pozo J, Hube M, Kurama Y (2021) Effect of material regularization in plastic hinge integration analysis of slender planar RC walls. Eng Struct 239(112302)
Ramos L, Hube M (2021) Seismic response of reinforced concrete wall buildings with nonlinear coupling slabs. Eng Struct 324
Rojas F, Suquillo B, Segura N, Bustos F, Díaz G, Diaz C, Carrillo J (2024) An experimental and numerical study of the response of rectangular wall systems coupled with reinforced concrete beams and slabs. In: Conference: 18th World Conference on Earthquake Engineering, Milan
Rossetto T, Gehl P, Minas S, Galasso C, Duffour P, Douglas J, Cook O (2016) Fracas: a capacity spectrum approach for seismic fragility assessment including record-to-record variability. Eng Struct 125:337–348
Saatcioglu M, Palermo D, Ghobarah A, Mitchell D, Simpson R, Adebar P, Hong H (2013) Performance of reinforced concrete buildings during the 27 February 2010 Maule (Chile) earthquake. Can J Civ Eng
Saito T, Kono S, Kusunoki K, Kim Y, Matsui T, Tani M, Gibu P (2011) Damage investigation of reinforced concrete buildings at the 2010 Chile earthquake. In: 8th International Conference on Urban Earthquake Engineering Proceedings, pp 679–681
Satake K, Heidarzadeh M (2017) A review of source models of the 2015 illapel, Chile earthquake and insights from tsunami data. Pure Appl Geophys 174(1)
Scott M (2019) portwooddigital. Retrieved September 18, 2024, from https://portwooddigital.com/2019/09/12/be-careful-with-modal-damping/
Scott M, Filippou F (2016) Hysteretic material. UC Berkeley, Oregon State University
Skarlatoudis A, Somerville PG, Thio HK (2016) Source-scaling relations of interface subduction earthquakes for strong ground motion and tsunami simulation. Bull Seismol Soc Am 4(106):1652–1662
TBI (2017) Tall buildings initiative, guidelines for performance -based seismic design of tall buildings. University of California, Berkeley
Thomsen JH (1995) Displacement based design of reinforced concrete structural walls: an experimental investigation of walls with rectangular and T-Shaped cross-sections. Clarkson University
TNO D (2017) Diana finite element analysis user manual (release 10. 2). Delft, The Netherlands
Ugalde D, Parra PF, Lopez-Garcia D (2019) Assessment of the seismic capacity of tall wall buildings using nonlinear finite element modeling. Bull Earthq Eng 17:6565–6589
Vásquez J, Heresi P (2024) Sesismic collapse risk assessment of T-Shaped reinforced concrete shear walls in Chile. In: 18th World Conference on Earthquake Engineering
Vásquez J, Jünemann R, de la Llera J, Hube M, Chacón M (2020) Three-dimensional nonlinear response history analyses for earthquake damage assessment: a reinforced concrete wall building case study. Earthq Spectra 37(1)
Wang J, Tan P, Huang T, He X, Zhou F (2024) Shear fragility analysis of non-classically damped three-dimensional structures under seismic excitation. Buildings 14(3967). https://doi.org/10.3390/buildings14123967
Westenenk B, de la Llera J, Jünemann R, Hube M, Besa J (2012) Seismic response of reinforced concrete buildings in concepcion during the 2010, maule earthquake. In: 15th World Conference on Earthquake Engineering
Wong P, Vecchio F, Trommels H (2013) VecTor2 and FormWorks User's Manual. 2nd edn.
Wu C, Peng Z, Ben-Zion Y (2010) Refined thresholds for non-linear ground motion and temporal changes of site response associated with medium-size earthquakes. Geophys J Int 182(3):1567–1576
Yassin M (1994) Nonlinear analysis of prestressed concrete structures under monotonic and cycling loads. In: University of California. Berkeley, PhD dissertation

Publisher's Note Springer Nature remains neutral with regard to jurisdictional claims in published maps and institutional affiliations.

Springer Nature or its licensor (e.g. a society or other partner) holds exclusive rights to this article under a publishing agreement with the author(s) or other rightsholder(s); author self-archiving of the accepted manuscript version of this article is solely governed by the terms of such publishing agreement and applicable law.

Authors and Affiliations

Javier Nebrijo[1,2] · Rosita Jünemann[1,2] · Tiziana Rossetto[3]

✉ Javier Nebrijo
janebrijo@uc.cl

[1] Department of Structural and Geotechnical Engineering, Pontificia Universidad Católica de Chile, Vicuña Mackenna 4860, Santiago, Chile

[2] Research Center for Integrated Disaster Risk Management (CIGIDEN), Vicuña Mackenna 4860, Santiago, Chile

[3] Department of Hydraulic Engineering, Technical University of Delft, Delft, Netherlands